

Simulation of the Radar Observation of a Sea Patch using the TLM Electromagnetic Method

Thibaut LURTON, Student Member IEEE, Christophe SINTÈS, Member IEEE and René GARELLO, Fellow IEEE

Institut Télécom – Télécom Bretagne UMR CNRS 2872 TAMCIC
Dept Image et Traitement de l'Information
29238 Brest Cedex, France
Email: thibaut.lurton@telecom-bretagne.eu

Abstract— We propose the simulated rendition of the observation of a variety of small sea patches by radar. These patches include a random sea surface of variable state, with possibly the presence of a manufactured, metallic object in its middle. The simulation in itself draws upon two different techniques which are combined: for the free-space propagation, a simple geometrical ray tracing method is used. On the other hand, we rely on a discrete calculation of the propagation of the electromagnetic waves in the vicinity of the sea surface, using the TLM method. Different aspects of this particular electromagnetic method are discussed in this paper. The originality of the approach is the combination of a geometrical calculation with a discrete, exact computation, each of them being devoted to a precise part of the simulation. Further matter in the article extends onto the explanation of some techniques developed for the need of our study, presentation and annotation of some results along with computation times, and overall discussion.

I. INTRODUCTION

The observation of the sea surface through the means of radars has many direct applications, the most numerous being considerations on the geophysical parameters (sea state, steepness of waves, roughness, currents, winds, etc.) What is more, the detection of objects in sea clutter, crucial as it is in certain fields, is an operation whose difficulty is directly related to the sea state, the radar characteristics, and the size of the spotted objects. A good knowledge of all this set of parameters is thus a key point to the mastering of the radar imaging of the ocean. In this paper, we perform a simulation of the radar observation of complex (i.e. including sea clutter and/or object) sea scenes on a small zone. The reason why we focus on a simulation process is the lack of general knowledge about the interactions between the radar electromagnetic wave and the different parts of a sea scene (waves, objects). Our work could yield clues about this prospective area of remote sensing.

The state of the art in the field of radar propagation simulation over the sea is quite diverse. It ranges from pure analytical methods [1], whose complexity is high, to semiempirical techniques [2], [3]. A good, comprehensive survey of the different methods encountered in the scientific literature can be found in [4]. Our approach will be based on a purely numerical simulation. We will expose throughout the article how we proceed to limit the weight of the calculation process.

The main idea in our simulation is to use a discrete, exact method to calculate the propagation of the radar electromagnetic fields. Because such methods are very heavy to implement due to the number of variables to handle, we have to restrain ourselves to a small portion of space. In this respect, we choose to define an area around the sea surface—where the reflection process arises—where the discrete calculation is performed. Out of this zone, the electromagnetic wave propagates in free space and therefore can be modeled by a simple ray-tracing method.

The electromagnetic propagation implementation retained is the TLM (Transmission Line Matrix) method, which will be described in paragraphs to come. Its efficiency for this particular type of problem is larger than similar methods such as the FDTD [5], and its capacity to integrate modules such as Perfectly Matched Layers [6] and to link bonds with the ray-tracing algorithms are much appreciated.

We have overall three main parts in our simulation program: first, the ray-tracing module, which operates on the largest zone of the studied space and is the lightest in terms of time of computation; then the TLM module, which performs the electromagnetic propagation calculation in the direct vicinity of the sea surface, in a very precise way but with large times of computation; finally, we use specific modules to transfer data from ray-tracing to TLM, and back.

We use this double-method algorithm to simulate the propagation of a radar signal from a single point in space to a defined patch of water, and back to the emission point (monostatic configuration).

In a first part, we will give details about how our simulation program is implemented. We will discuss a certain number of points which had to be solved during our study, then we will go through some specific simulations we achieved and the appended results, and we will conclude with a discussion regarding the efficiency of the method.

II. DESCRIPTION OF THE SIMULATION PROGRAM

Three parts will be detailed, corresponding to the three main modules of our program. First, the ray propagation device, then the TLM computation module, and finally the linking between the two.

A. Ray tracing

Our method to propagate electromagnetic waves through free space is really basic. It is sheer geometrical propagation, with no reflection since no obstacle is encountered. Therefore, it only consists in a phase adaptation and a spheric divergence amplitude factor.

In a first step, we perform a projection of the rays from the source point to the discrete area enclosing our sea patch. To each of the points needed to initiate the fields in the TLM zone we affect an amplitude factor and a phase corresponding to a straight line propagation. At any time of the TLM computation, initiating fields can be easily derived from those data and the waveform. With this projection method, any waveform can be used in the process, and we do not have to reiterate the projection at each temporal step of the TLM run, which constitutes an appreciable gain of time.

Because of the symbolic nature of the calculation performed, any distance can be considered from the radar to the TLM zone. Defining a radar object carried by an airplane or by a satellite will not make any difference in terms of computation times.

B. The Transmission-Line Matrix (TLM) method

Regarding the discrete computation, we use the TLM method. This technique is widespread for antenna studies in the microwave field, and was invented in the 1970s by Johns and Beurle [7]. It is a cousin method to the FDTD technique, being both discrete in time and in space; the main difference is that the FDTD method relies on the linear approximation of derivatives, whilst the TLM method is based on the electromagnetic equivalence between a virtual mesh in space and lines of currents (hence its name).

This paper does not aim at comprehensively presenting the TLM method, as its theory is complex. The study we propose draws upon previous works led at Telecom Bretagne [8], [9] to which the reader can refer for further explanation. We will limit ourselves to a rapid overview of the method.

The TLM spatial mesh consists in elementary nodes, arranged on a Cartesian grid, each of which possessing six “arms” that bond with the surrounding other nodes in the three dimensions. The TLM method runs as a basic algorithm of energy exchange between nodes through their arms: at every temporal step, transfers of energy are operated from one node to another, considering their own permittivity, the presence of electromagnetic frontiers between them, etc. It can be seen as a “stand-alone” process, as no outside intervention is needed: for example, if we define a reflecting electromagnetic plane on certain cells and initialise an incident field upon it, the energy will propagate “by itself” from node to node, and the TLM method will naturally produce the physical response of the scene awaited, i.e. a reflection of the incident wave.

C. Switching from ray-tracing to TLM and back

The adaptation of the two methods described in the previous paragraphs is performed through the use of particular elements of the electromagnetic theory, some virtual surfaces on which

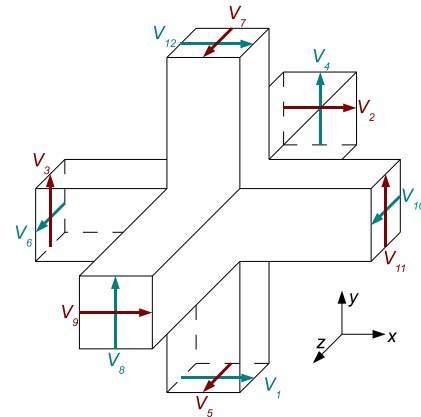


Fig. 1. TLM elementary node, with its six arms and twelve voltages transferring energy.

the field values are considered in order to process calculation. There are two of these surfaces: the *Huygens* surface is used to initiate the field values inside the TLM zone, whereas the *Kirchhoff* surface is used for an integration of the local electromagnetic fields, yielding the value of any component of the electromagnetic field in any point of space, which is useful whenever we want to calculate our backscattered signal.

How the Huygens surface works is really simple: it merely consists in an initialisation of field values through the projection process we saw previously. The Huygens surface is a virtual box (theory states it has to be closed) on the side of which electromagnetic values are defined at each TLM step. These values are transmitted step after step from node to node, thus feeding the whole grid with incoming energy.

As for the Kirchhoff surface, its theory is slightly more difficult, as it induces the use of discrete integral calculation. We shall not enter into details. Basically, the algorithm gathers the values of fields and derivatives on a box-shaped area enclosing the Huygens box, and derives from those the field value in a given point, which can be located in either near or far field zone. This calculation can be performed at any temporal step, and therefore fields can be monitored throughout time.

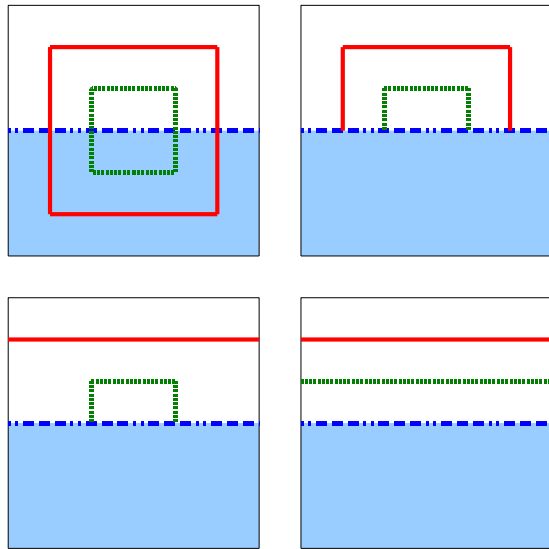
The use of both the Huygens and Kirchhoff surfaces in link with the TLM method was fully validated at Telecom Bretagne’s Microwave Department [8].

III. IMPLEMENTATION OF THE SIMULATION

In this section, we will go through a certain number of points that have to be cleared before any simulation is led. Though it may seem technical, this part was written to enlighten how several problems were dealt with in our study, and notably how some solutions helped simplifying the whole simulation process.

A. Discussion over the shape of Huygens’s and Kirchhoff’s surfaces

As we briefly saw in the previous section, there are theoretically three major conditions to fulfill in the use of Huygens’s and Kirchhoff’s surfaces:



— Kirchhoff's surface ····· Huygens's surface
 ······ Sea/air interface

Fig. 2. Four proposed configurations for the disposal of Huygens's and Kirchhoff's surfaces.

- 1) Kirchhoff's surface must encompass Huygens's surface;
- 2) Kirchhoff's surface must contain all electromagnetic sources of the problem;
- 3) the surfaces have to be closed.

These conditions yield difficulties with our scheme. First, assuming that our two Huygens's and Kirchhoff's surfaces contain the (secondary) sources of the problem—i.e. the surface of the sea—, then one can see that the sides of the surfaces have to cross the water/air interface. At this point, we should note that no development in the theory of Huygens's surface yet allows us to declare fields in two mediums simultaneously. It is simply out of bounds regarding the state of the art of the electromagnetic theory today. The same problem arises with Kirchhoff's surface. Therefore, we cannot use box-shaped surfaces (figure 2 top left) and we will have to work with open surfaces. Those will be approximations, and we will have to ensure they provide with good results.

A first guess would be to use cup-shaped surfaces (figure 2 top right), with Kirchhoff's surface still enclosing Huygens's surface. This configuration should not be too remote from the "box" configuration, since the penetration of waves in the water medium is very shallow at high frequencies. Anything happening below the air/water interface should then be negligible.

The problem with this configuration is that we have to ensure that the sides of the cups strictly follow the geometry of the surface: a cell-to-cell spatial adaptation has to occur so that no space is left between the edge of the cup and the air/water interface, and so that the edge does not penetrate into water either. If the sea surface is rough, then the side panel of the cup will have to be cut out accordingly. This can be

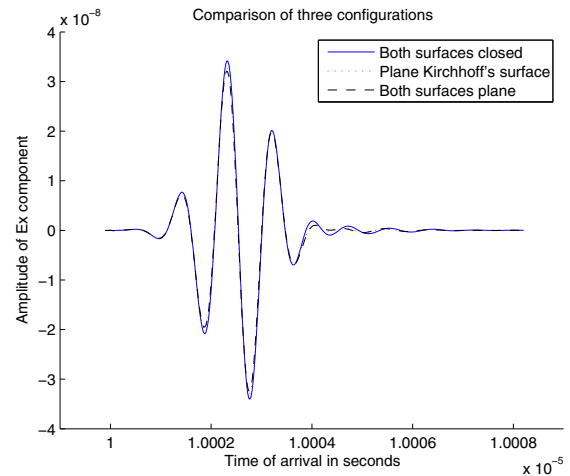


Fig. 3. Comparison of the responses of three of the detailed configurations.

heavy to implement. As a solution, we propose the use of flat surfaces (figure 2 bottom). They are indeed extensions of the cup configurations, as if the horizontal dimensions of the cup were infinite.

As we can see, the flat surfaces are the simplest configuration, as they require the handling of one side only.

The graph shown on figure 3 displays the responses of three basic scenes including a flat electromagnetic mirror to the same excitation signal, the differences bearing on the setting up of Huygens's and Kirchhoff's surfaces. A remarkable agreement is found between the three response plots, demonstrating that the geometry of Huygens's and Kirchhoff's surfaces is indeed flexible.

For the sake of simplicity, we decided to use flat surfaces for both Huygens's and Kirchhoff's in the rest of our study.

The next paragraph deals with the overall number of nodes and its link to the efficiency of computation.

B. Sizing the number of nodes

As for any numerical method, there are some constraints on the size of the TLM nodes. Namely, the grid should sample space at a period smaller than $\lambda_{min}/10$ or $\lambda_{min}/8$ depending on the acceptance—we will stick to $\lambda_{min}/10$ —, where λ_{min} is the smallest wavelength emitted. As an example, working at 10 GHz would yield a spatial increment of $\delta l = 3$ mm. Now, this relation has to include a supplementary parameter when the TLM space contains different mediums. We have then:

$$\delta l = \frac{\lambda_{min}}{10\sqrt{\epsilon_{max}}} \quad (1)$$

where ϵ stands for the relative permittivity. For sea water, we can easily expect the $\sqrt{\epsilon_{max}}$ term to be of a few unities. Considering again our example at 10 GHz, we have $\epsilon \approx 50$, and so $\delta l \approx 4.3 \times 10^{-4}$ m. The division of the spatial increment finds an echo at the power of three in the total number of nodes (here, multiplication by ≈ 350).

As we can see, the presence of sea water entails tiny cell sizes, and leads to cumbersome numbers of nodes on a whole

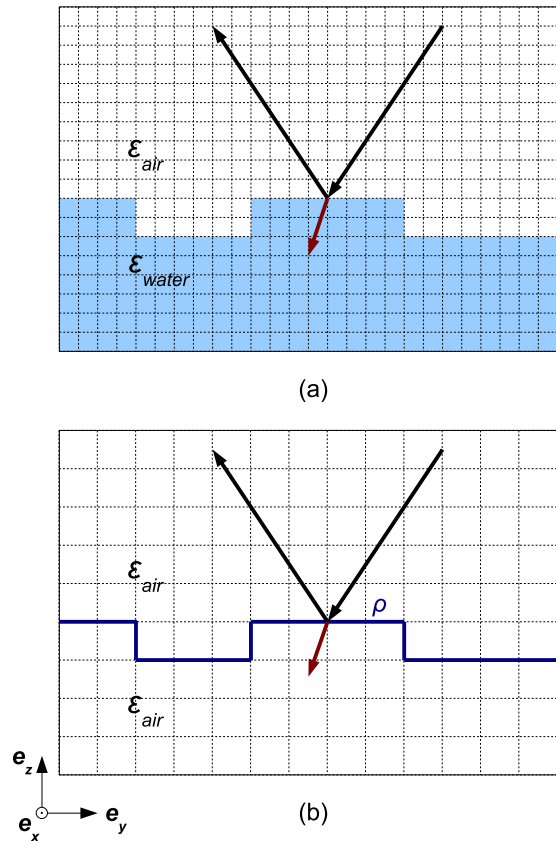


Fig. 4. Comparison of the two solutions proposed for the spatial meshing. (a) Comprehensive meshing, with water and air blocks. (b) Lighter meshing, with presence of an electromagnetic frontier. Arrows depict incident/reflected/refracted waves.

area. The method we are exposing in the next paragraph allowed us to reduce the number of nodes and therefore to save computation time.

The basic idea in our node-reducing principle is the equivalence between the air/sea interface and an electromagnetic frontier as can be defined between two TLM nodes. Figure 4 shows the meshing of the same volume of space, including a simulated sea patch, in two different ways: in the first method, two blocks of materials are defined, one whose permittivity is 1 (air) and the other whose permittivity is ϵ_w (water). Because of the presence of this block of water, the whole space has to be meshed with a spatial period of $\lambda_{min}/10\sqrt{\epsilon_w}$, so on a thinner grid than if it had been air alone. The reflection process at the interface between the blocks of air and of water will occur as an inherent part of the TLM propagation algorithm. In the second method, both blocks are considered to be constituted of air. The limit between water and air is modeled by an electromagnetic frontier to which a certain reflection factor ρ is assigned to produce reflection. In this scheme, the meshing can be loosened to $\lambda_{min}/10$ because no water block is involved anymore.

In the configuration where an electromagnetic frontier is used, each of the boundary nodes must be given a reflection

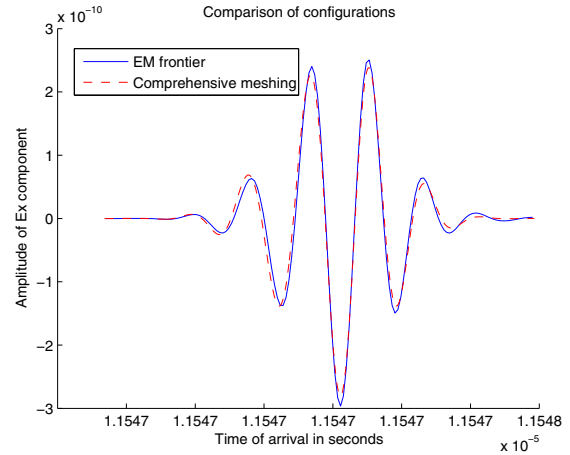


Fig. 5. Comparison of the response of the two solutions proposed for the spatial meshing.

factor. Sea water does not constitute a perfect electromagnetic mirror. Therefore, its reflection factor is not purely (-1) . What is more, the reflection is affected by the angle of incidence of the electromagnetic wave on the water surface. Thus we have to consider the incidence angle between the illumination direction and every facet of the air/sea electromagnetic interface. (Note that this incidence angle is not the same depending on whether the facet we are dealing with is on the top of a node, or on one of its sides.) We relied on the tables given in [10] for an estimation of the sea water reflection factor of an electromagnetic wave at a given frequency and with a defined incidence angle. Those values are *reflection factors*, i.e. given for one incidence angle and its equal reception angle. A slight, simple trigonometry correction is needed to adapt the factor to our case, where the Cartesian TLM grid makes energy travel along the axes.

The graph displayed in figure 5 shows a comparison between two signals issued from the same scene, including a small mirror enlightened by a 30° -incident electromagnetic wave. What is measured is the far-field response of the mirror through time. The difference between the two signals is the method adopted for the spatial meshing. One simulation was carried out using comprehensive meshing, and the other using an electromagnetic frontier. Concordance between the two simulations is found to be good. We conclude that, as both methods are equivalent, we can freely choose to use the lighter to perform our computations (i.e. the configuration with the electromagnetic frontier).

C. Scene generation

In order to implement a sea surface within our discrete TLM zone, we have to generate the shape of the interface. The method we retained is a spectral one. It is based on the works by Elfouhaily et al. [11], and the main idea is that a random sea surface can be described by the means of its power spectrum, which varies as k^{-4} , k being the wave-number. A variety of directional functions are available to give our sea

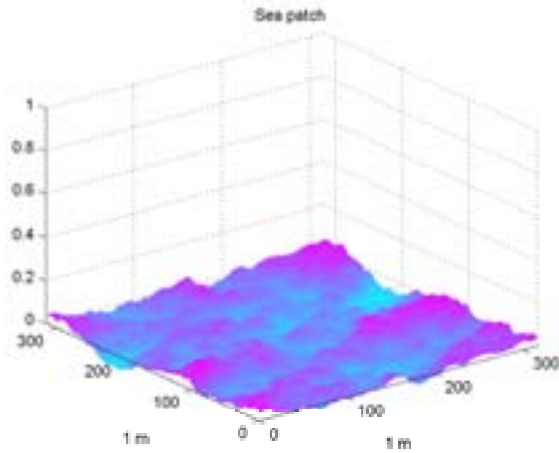


Fig. 6. An example of the generation of a sea surface using Elfouhaily's spectrum.

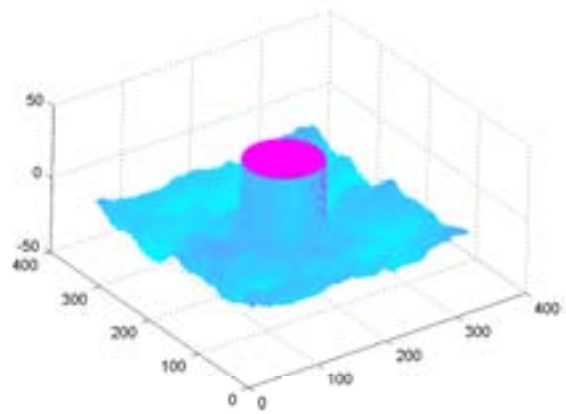


Fig. 7. Illustration of the configuration including sea surface and a cylindrical, metallic object on surface.

state an alignment regarding the propagation of waves.

Figure 6 shows an example of a small sea patch generated through the use of Elfouhaily's spectrum.

Once the sea surface has been generated, it is easily imported into the TLM mesh (as it is already a discrete surface) and translated in terms of elementary frontier facets. Each of the facets is then given a particular reflection coefficient.

The inclusion of an object within the scene is done in a much similar way to the generation of the sea surface: the given surface is then geometrical (sphere, cylinder, cube...), and the reflection coefficient is set to (-1) for the generic case of a metallic object.

The next part will detail the setting up and results of a few simulations.

IV. SIMULATIONS

The current section presents a bunch of simulations carried out using the whole program. We worked on 1 m^2 -patches of sea, and illuminated them with a 45° -incident, VV-polarised, X-band signal (9.5 GHz carrier shaped by a 0.3 ns-wide Gaussian) issued from a point at altitude 3000 m. We chose to generate a calm sea patch, an agitated sea patch, and a patch with medium sea conditions including a cylindrical, metallic object on the surface (figure 7).

A. Response graphs

Figures 8, 9 and 10 show the electromagnetic response through time of the three scenes we simulated. One can notice a coherent signal backscattered from the first two scenes (sea only), with a higher level of energy and a greater signal-to-noise ratio for the agitated sea. This is due to specular reflection, as more facets are likely to reflect energy toward the radar in the second configuration. As for the third graph, the signal is much more complex.

From these graphs, backscattering cross section of the patch observed can easily be derived.

To this end, we will consider the amplitudes of the signals. The emitted signal in our simulations was normalised to a

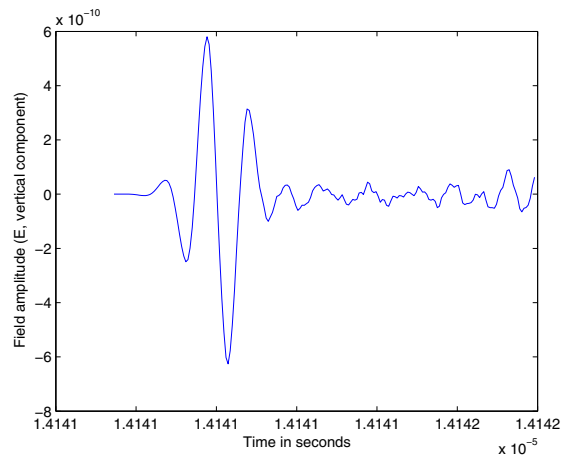


Fig. 8. Response of the calm sea patch.

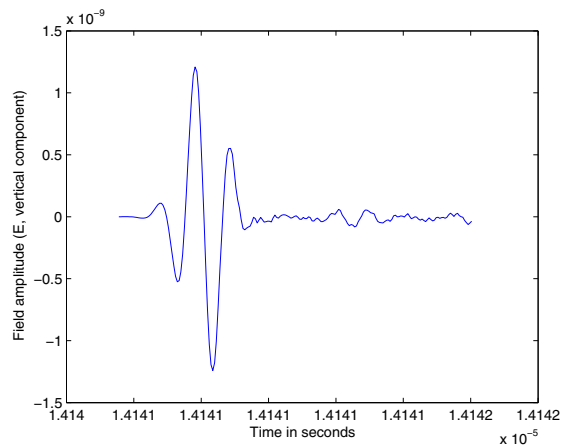


Fig. 9. Response of the agitated sea patch.

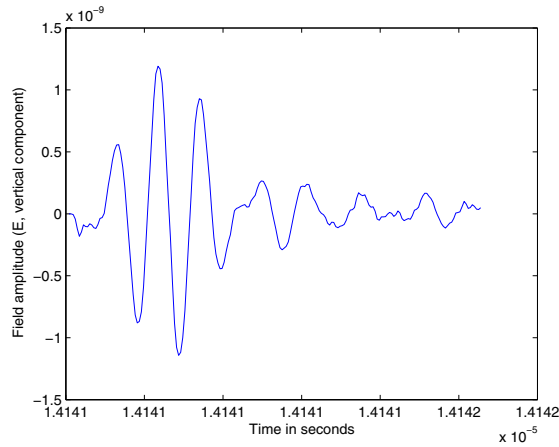


Fig. 10. Response of the sea patch including an object.

TABLE I
BACKSCATTERING CROSS SECTION

	Backscattering cross section (dB)
Calm sea	-15.7
Agitated sea	-9.3
With object	-10.1

peak amplitude of $1 \text{ V}\cdot\text{m}^{-1}$; as for the received signals, the maximum amplitude E_r can be read on the corresponding graphs. The patches observed are of area 1 m^2 , however in order to obtain the normalised backscattering cross section we must consider the instantaneous illuminated area, given by:

$$A = \frac{cT}{2 \sin \theta} \times 1 \quad (2)$$

T being the length of the signal (0.3 ns) and θ the incidence angle. We find $A = 0.0636 \text{ m}^2$.

The normalised backscattered cross section is then:

$$\sigma^0 = 20 \log(E_r R^2) + 10 \log\left(\frac{4\pi}{A}\right) \quad (3)$$

Our calculations are reported in table I. We can compare these values to those found in papers such as [12], and find that the order of magnitude is in fair agreement with the theory.

As can be noticed in table I, the backscattering cross section is stronger for an agitated sea than for a calm sea. Indeed, under our 45° incidence, a calm and flat sea provides with less facets reflecting the energy toward the sensor. With the sea state growing, this number of specular reflectors rises, enhancing the response of the sea patch.

As for the backscattering coefficient of the third scene, the cross section is comparable to the second case. One could object that a stronger response could have been awaited because of the presence of the metallic object. We can explain this value by the fact that, because of its shape, the metallic object presents indeed few facets to reflect the signal back to the emission point.

TABLE II
COMPUTATION TIMES

	Scene size	Number of nodes	Run time
Calm sea	$346 \times 346 \times 90$	10 774 440	46 min
Agitated sea	$346 \times 346 \times 140$	16 760 240	1 hr 19 min
With object	$346 \times 346 \times 130$	15 563 080	1 hr 4 min

B. Computation times

Table II sums up the computation times needed to perform our calculations. The patches were observed over 200 TLM iterations. All calculations were carried out by a standard workstation clocked at 2.4 GHz with 4 GB RAM.

As we can see, computation times are quite important, though not cumbersome. Note that we chose the X-band for the realism of the simulation. Changing it to L-band for example would loosen drastically the mesh, and therefore lead to much more efficiency in the computation, with run times of one to two minutes only.

V. DISCUSSION

The work on the backscattering cross section coefficients is on its beginnings. We saw that the first results were quite satisfactory, however, some more development is awaited, for example for simulations with different angles of incidence in order to check whether or not accordance with the reflection theory is still verified.

Some technical points within the simulation are still matter of discussion. In particular, because we have to affect a given incident angle to every facet of the electromagnetic frontier, multiple rebounds (i.e. with a changing incident angle) cannot be modeled accurately. We will have to estimate whether this issue can be neglected or not.

As for computation times, our performances are reasonable, depending on the size of the patch we want to observe. We saw that working with lower radar frequencies could speed up the process and give faster times than those exposed in this article.

VI. CONCLUSION AND PERSPECTIVES

In this paper, we have shown the possibility of linking ray tracing calculation to a discrete, local computation of electromagnetic fields in order to simulate the propagation of a radar wave. Thanks to the TLM method, inherited from the microwave domain, and with the use of a few technical tricks that have been detailed throughout the article, we can achieve fairly acceptable times of computation and obtain the simulated response of small sea patches to an incident radar wave. An idea for further development is for this kind of signals to be gathered in a sort of bank of generic responses, which would be classified by sea-state, slope, surface composition, etc. Any large-size rendition of a sea surface could then be divided into small patches, and each of them associated with the corresponding generic response. This way, a map of reflectivity of a large zone illuminated by a radar could

be rapidly derived. The main issue arising would be energy exchange between the defined patches.

Further processing such as the collection of many illuminations so as to form a synthetic aperture image is theoretically possible, though achievable with difficulty for the moment because of computation times. We shall be working on this type of up-level processing.

As for speeding up the process, several ways could be proposed. In our study, though we used some cell loosening, we restrained ourselves to a comprehensive meshing of space. A large number of nodes though are not vital to the process, for example those situated under the sea surface. The development of an adaptive, non-parallelepipedic zone of calculation could lighten the computation.

ACKNOWLEDGEMENTS

We whole-heartedly thank Dr. Jérémy Lanoë and Dr. Sandrick Le Maguer from Telecom Bretagne's Microwave department, who provided with most of the basic material for the programming of the TLM implementation. Finally, we would like to thank the Brittany Region for supporting this study through a PhD grant.

REFERENCES

- [1] A. G. Voronovich, *Wave Scattering from Rough Surfaces*. Berlin, Heidelberg, New York, Londres, Paris, Tokyo, Hong Kong, Barcelone, Budapest: Springer-Verlag, 1994.
- [2] V. Kudryavstev, D. Hauser, G. Caudal, and B. Chapron, "A semiempirical model of the normalized radar cross-section of the sea surface

1. background model," *Journal of Geophysical Research*, vol. 108, pp. FET2.1–FET2.24, Jan. 2003.
- [3] V. Kudryavstev, D. Hauser, G. Caudal, and B. Chapron, "A semiempirical model of the normalized radar cross-section of the sea surface 1. radar modulation transfer function," *Journal of Geophysical Research*, vol. 108, pp. FET3.1–FET3.16, Jan. 2003.
- [4] T. Elfouhaily and C.-A. Guérin, "A critical survey of approximate scattering wave theories from random rough surfaces," *Waves Random Media*, vol. 14, pp. R1–R40, Aug. 2004.
- [5] Th. Lurton, Ch. Sintès, R. Garelllo, and D. Guériot, "A simulation of the synthetic aperture radar observation of a manufactured object in sea clutter using finite differences," *IEEE Conference OCEANS 2007, Vancouver*, pp. 1–6, 2007.
- [6] J.-P. Béranger, "A perfectly matched layer for the absorption of electromagnetic waves," *Journal of Computational Physics*, vol. 114, pp. 185–200, Oct. 1994.
- [7] P. B. Johns and R. L. Beurle, "Numerical solution of 2-dimensional scattering problems using a transmission-line matrix," *Proceedings IEE*, vol. 118, pp. 1203–1208, Sept. 1971.
- [8] N. M. Peña Traslavina, *Contribution au développement de conditions aux limites absorbantes pour la méthode TLM avec applications à l'analyse de circuits hyperfréquences*. PhD thesis, Université de Rennes I, Dec. 1997.
- [9] J. Lanoë, *Contributions au couplage entre la méthode TLM et la théorie physique de la diffraction pour l'analyse électromagnétique d'antennes dans leur environnement*. PhD thesis, Université de Bretagne Occidentale, Feb. 2008.
- [10] L. Boithias, *Propagation des ondes radioélectriques dans l'environnement terrestre*. Paris: Dunod, 2 ed., 1984.
- [11] T. Elfouhaily, B. Chapron, K. Katsaros, and D. Vandermark, "A unified directional spectrum for long and short wind-driven waves," *Journal of Geophysical Research*, vol. 102, pp. 15781–15796, July 1997.
- [12] G. R. Valenzuela, "Theories for the interaction of electromagnetic and oceanic waves - a review," *Boundary-Layer Meteorology*, no. 13, pp. 61–85, 1978.